Gilbert damping of CoFe-alloys

Ramon Weber[1], Dong Soo Han[1], Isabella Boventer[1, 2], Samridh Jaiswal[1, 3], Romain Lebrun[1], Gerhard Jakob[1], and Mathias Kläui[1]

[1] *Institute of Physics, Johannes Gutenberg University Mainz, 55099 Mainz, Germany,*
[2] *Institute of Physics, Karlsruhe Institute of Technology, 76131 Karlsruhe, Germany,*
[3] *Singulus Technologies AG, 63796 Kahl am Main, Germany*

(Dated: January 9, 2019)

Abstract

We report structural, magnetic and dynamic properties of polycrystalline Co_xFe_{1-x}-alloy films on Sapphire, Silicon and MgO substrates across the full composition range, by using a Vector Network Analyser ferromagnetic resonance measurement technique (VNA-FMR), Superconducting Quantum Interference Device magnetometry (SQUID) and X-Ray Diffraction (XRD). In the approximate vicinity of 28% Co, we observe a minimum of the damping parameter, associated with a reduction in the density of states to a minimum value at the Fermi energy level. For films on all substrates, we find magnetic damping of the order of $4\text{-}5\cdot10^{-3}$, showing that the substrate does not play a major role. Using a post-annealing process, we report a decrease of the magnetic damping down to $3\text{-}4\cdot10^{-3}$. We find that the saturation magnetization depends approximately reciprocally on the damping parameter with varying alloy composition.

I. INTRODUCTION

One of the primary goals of research in the field of magnetic memory technology is to create a non-volatile memory that is both, faster and more robust than conventional random access memory types (RAM). Magneto-resistive RAMs (MRAMs) are considered as promising candidates, which already have commercial applications[1–3]. MRAMs are usually based on magnetic tunnel junctions (MTJs), which can be used in spin-transfer torque devices. In such devices spin-polarized electron currents can be used to switch the magnetization of a ferromagnetic layer in a spin valve structure, which is measured by the

change of the resistivity[4, 5]. It is known that the critical current at which the free layer of the junction will switch direction is for spin-transfer torque switching in the conventional geometry proportional to the Gilbert damping parameter of the ferromagnetic material[6]. Hence, for further progress in MRAM technology the minimization of Gilbert damping in such systems is crucial.

A low Gilbert damping parameter also enhances the speed of magnetic solitons such as domain walls (DW), where the DW-velocity is inversely proportional to the Gilbert damping parameter beyond the Walker breakdown and therefore low damping increases the speed of wall displacement[7, 8]. In the case of topological stable solitons like skyrmions, tuning the damping constant in different directions can confine the skyrmion motion to the racetrack center to avoid annihilation of skyrmions at the edges[9]. In spin-torque oscillators, low magnetic damping also improves the spectral coherence of the oscillator[10] and their mutual synchronization properties[11]. Ultimately, the diffusion of spin currents is known to be inversely proportional to the Gilbert damping[12, 13], which is of primordial importance for spintronic devices[14].

So far, the lowest values regarding Gilbert damping in magnetic materials have been observed in insulators, namely in Yttrium Iron Garnet (YIG) with values of around (10^{-5}) [15, 16]. However, magnetic insulators cannot be used for applications where a charge current is required. One proposed alternative class of materials with low Gilbert damping are Heusler alloys, which entail challenging fabrication processes. Recently, a new perspective has emerged with the observation of ultra-low Gilbert damping in 10 nm thick polycrystalline cobalt-iron (Co_xFe_{1-x}) alloys grown on silicon (Si) substrate[17]. An ultra-low damping with an effective value of $(2.1 \pm 0.1) \cdot 10^{-3}$ was found for a composition of about 25 % of Co as predicted in 2010 by Mankovsky *et al.* [18]. While they assumed that bulk-like Gilbert damping dominates, a modified interface electronic structure was not considered. They obtained a minimum of Gilbert damping between 10 % to 20 % of Co, which was not observed experimentally yet. Turek *et al.* predicted a minimum of Gilbert damping at 25 % in their theoretic work[19]. In experiment, the calculation leads to an intrinsic Gilbert damping value of $(5.0 \pm 1.8) \cdot 10^{-4}$ in out-of-plane (OOP) geometry[17].

Similar Gilbert damping values for Co_xFe_{1-x}-alloys in in-plane (IP) geometry were reported latterly. While Körner *et al.* found an effective value of $\alpha_{eff} = (3.9 \pm 0.3) \cdot 10^{-3}$ for a composition of 25 % Co grown by Molecular Beam Epitaxy (MBE)[20], Lee *et al.* have reported effective Gilbert damping values lower than $1.4 \cdot 10^{-3}$ for epitaxial films[21].

In our work, we measure the damping of polycrystalline Co_xFe_{1-x}-alloys grown with an industrial sputter tool on 8" wafers. In line with previous results, we confirm that low Gilbert damping can be obtained in polycrystalline Co_xFe_{1-x}-alloys and we show that these results are robust as they can be obtained for samples grown on various substrates such as Si, MgO and Al_2O_3 in in-plane magnetization configuration. We observe a minimum of the Gilbert damping parameter at approximately 28 % of Co. By annealing the metallic films, we demonstrate that we can further reduce the magnetic damping, which we attribute to the enhanced crystallinity of our films after the heat treatment.

II.SAMPLES AND MEASUREMENT METHODS

The Co_xFe_{1-x} alloy thin films are deposited on three different substrates namely thermally oxidized Si (001) coated with approximately 100 nm of SiO_2, Al_2O_3 $(11\bar{2}0)$ and MgO (001) using a *Singulus Rotaris*® Ultra-High Vacuum (UHV) deposition system with a base pressure of less than 10^{-8} mbar. A 3 nm-thick Ta seed layer is deposited onto the substrates prior to the growth of Co_xFe_{1-x} to improve adhesion of the subsequently followed Cu film[22]. The Cu interlayer suppresses interfacial intermixing between Co_xFe_{1-x} and Ta[4] and helps thus to grow Co_xFe_{1-x} with low damping[4, 23, 24]. The films are grown by co-sputtering from Co and Fe targets, whilst manipulating sputtering rates of each target to obtain the desired composition. On top of the Co_xFe_{1-x}, Cu and Ta layers are repeatedly deposited to allow symmetrically layered structures that suppress the contribution from other effects, e.g. spin pumping and inverse spin Hall effect, to the Gilbert damping constant and provide protection against oxidation. To summarize, the complete stack is comprised of substrate/Ta(3 nm)/Cu(3 nm)/Co_xFe_{1-x}(10nm)/Cu(3nm)/Ta(3nm).

After deposition, we performed for some samples a post-deposition annealing process at 530 °C (heater temperature) for one hour for selected compositions[25] to explore possible additional approaches to reducing the Gilbert damping constant.

The damping parameters of Co_xFe_{1-x} are measured by a Vector Network Analyzer-Ferromagnetic Resonance (VNA-FMR) setup in a two-port transmission configuration. A 50 Ω matched Coplanar Waveguide (CPW) with a 330 μm - wide transmission line is used to apply oscillating microwaves to the samples. In-plane bias fields in the range of 20 - 180 mT are applied parallel to the transmission line, wherein the in-plane microwave field is transverse to the magnetization. The standard microwave scattering parameters (S-parameters) are collected from the vector network analyzer (Rohde & Schwarz VNB20), while sweeping the frequency of the microwaves from 100 kHz to 20 GHz with in-plane bias fields. The absorption of the microwave signal is reflected to the impedance as well as the susceptibility of the device under test[26]. To examine the frequency and field dependence of the susceptibility of the samples, we employed a two-port evaluation scheme by Barry *et al.*[27], where the effective microwave permeability parameter U for a given frequency f and in-plane field H is given by:

$$U(\omega, H) = \pm \frac{\ln\left[\frac{S_{21}(\omega,H)}{S_{21,ref}(\omega,H_{ref})}\right]}{\ln\left[S_{21,ref}(\omega,H_{ref})\right]} \quad (1)$$

Here, S_{21} is a scattering coefficient which represents transmission of the signal from port 2 to 1. $S_{21,ref}$ indicates the S_{21} parameter measured at a reference field, i.e., in our case at $\mu_0 H$ = 650 mT.

In measurements where we fixed the external magnetic field H at different values and swept the frequeny ω a loss of signals, frequency dependent and constant in field, and a phase lag between two components of the complex S_{21}-parameter occurs, which is mostly attributed to the change of the propagation characteristics of the waveguide by external excitation frequencies. Thus we fitted the measured S_{21}-parameter $\tilde{S}_{21}(H)$ to the following equation:

$$\tilde{S}_{21}(H) = S_0 + \frac{A}{H_{res}^2 - H(H - i\Delta H)} \cdot e^{-i\phi} \quad (2)$$

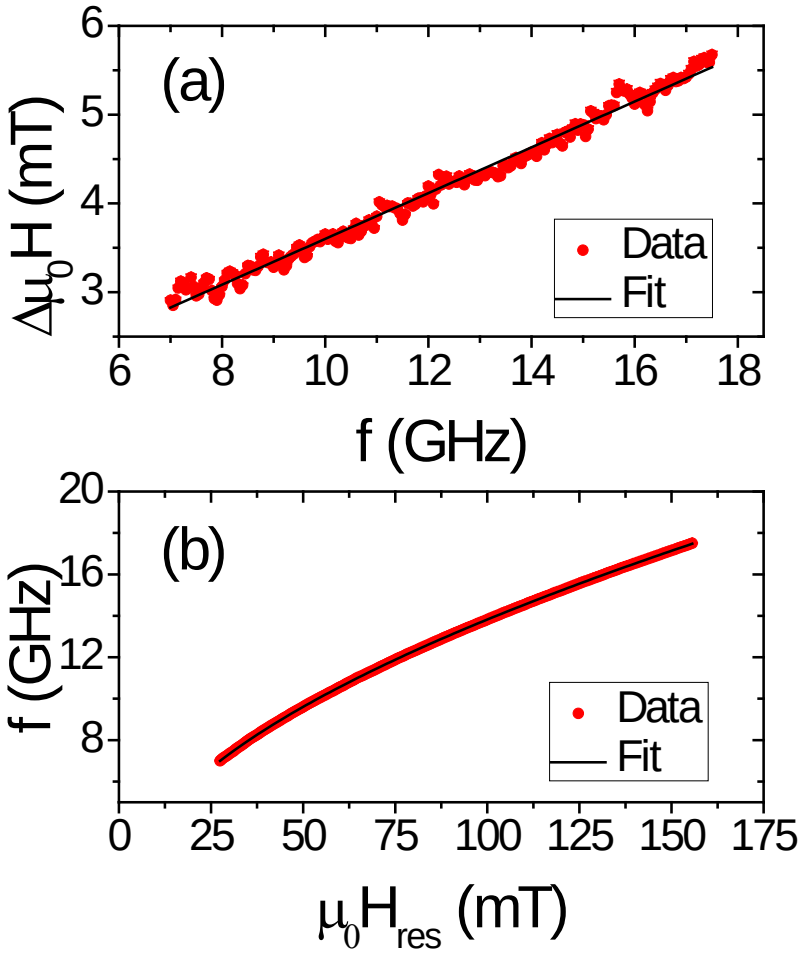

Figure 1: (a) Measured linewidth dispersion and (b) resonance field of Co_xFe_{1-x} grown on Si substrate with 28% Co after annealing. Data is represented in red, whilst the data in (a) are fitted by equation (4) and in (b) are fitted by equation (3).

Here A and ϕ are fitting parameters, which represent the offset and phase shift of the signal. H is an external magnetic field. H_{res} and ΔH are the magnetic field at resonance and the linewidth of FMR peak, respectively. The sign is chosen to be negative for Im[U(H)] in the vicinity of the FMR peak. We note that, for the analysis of the damping, we used the evolution of U as a function of H to get the linewidth of resonance peaks[28, 24]. This allows us to determine the Gilbert damping parameter reliably even for the case with a large zero-frequency intersect in ΔH vs. f. Fig. 1b shows the field dependence of the FMR frequencies as obtained from the analysis of U vs. H. For example, it shows the result for $Co_{28}Fe_{72}$ thin film

grown on the Si substrate and post-annealed. The f versus H is fitted to the Kittel equation for thin films, which is expressed as:

$$f = \frac{|\gamma|\mu_0}{2\pi}\sqrt{(H_{res} + H_k + M_{eff})(H_{res} + H_k)} \quad (3)$$

The uniaxial in-plane anisotropy H_K and the effective saturation magnetization M_{eff} are estimated by fitting the data to equation (4). For the FMR analysis, the gyromagnetic ratio corresponding to the value for an electron[27], is assumed for all samples. $M_{eff} = M_S - \frac{2K_{u,\perp}}{\mu_0 M_S}$ is the effective demagnetizing field associated with shape anisotropy and out-of-plane anisotropy energy constant $K_{u,\perp}$. H_{res} describes the in-plane bias magnetic field at resonance, and H_k corresponds to the in-plane anisotropy constant.

Fig. 1a shows the ΔH as a function of f. It is shown that ΔH vs. f shows the expected linear dependence indicating Gilbert damping plays a key role. The effective Gilbert damping constant can be extracted from the following equation:

$$\Delta H = \frac{4\pi\alpha_{eff}}{|\gamma|\mu_0} f + \Delta H_0 \quad (4)$$

Here, α_{eff} is the effective Gilbert damping parameter and anti-proportional to the gyromagnetic ratio γ with a zero-frequency intersect ΔH_0, also known as residual linewidth. The saturation magnetization and the magnetic anisotropy were measured by using a SQUID magnetometer at room temperature. The crystalline structure of the thin films is examined by X-Ray Diffraction (XRD). The deposition conditions are optimized based on X-Ray Reflectometry (XRR) measurements which allowed us to determine the interface roughness and at the same time we obtain the thickness of the films.

III. RESULTS

The first experiment we present is based on investigating the Gilbert damping constants of different Co_xFe_{1-x}-alloy composition grown on different substrates. As shown in Fig. 2, the

damping of the alloys has a minimum for Co concentrations between 18 to 32 %. No significant difference in the magnitude of the damping parameters nor on the range of the measurement accuracy is observed for growth on different substrates. The error bars stem from the standard errors of the fits, repeatability and the maximal change of the gyromagnetic ratio. For the fits, we used the constant ratio of an electron[29, 30], which means that we have an additional, strictly positive contribution, i.e. leading to an additional error

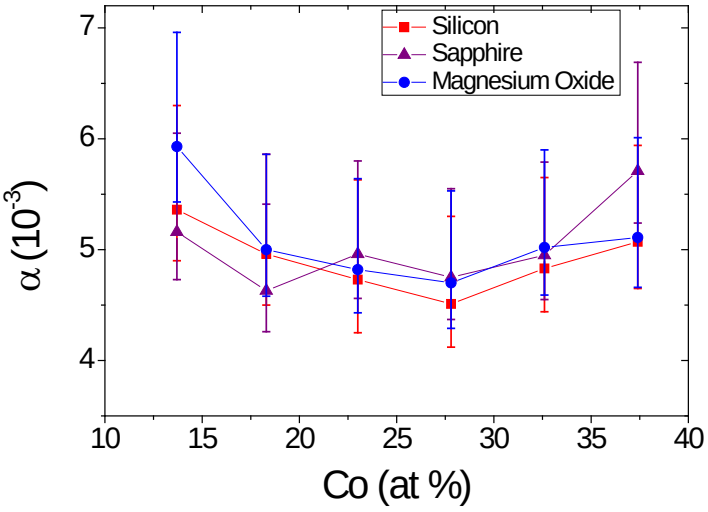

Figure 2: Comparison of the Gilbert damping parameters of Co_xFe_{1-x} -alloys grown on different substrates as a function of composition, extracted by a linear regression of equation (5).

of the measured Gilbert damping. We report here effective Gilbert damping below $5 \cdot 10^{-3}$ for all three types of substrates. The observation of low magnetic damping in the same composition range of Co_xFe_{1-x} for different substrates confirms that it originates from electron-magnon scattering as predicted by Mankovsky *et al.* with a dominating bulk-like Gilbert damping contribution[18].

In the following, we discuss the different contributions to the total linewidths and the role of the zero frequency linewidth. There exist two main damping channels: the Gilbert type, where the energy is directly transported to the lattice and non-Gilbert-type damping, which corresponds to a transition of uniform spin waves with $k = 0$ to non-uniform spin waves of different modes with $k \neq 0$, dissipating their energy to the lattice in an indirect way. In most cases the standard linear Gilbert model is used, due to its linear dispersion of the linewidth.

More general models for the determination of dynamical parameters were developed, including nonlinearities of the relaxation process in which the linewidth consists of four different parts[31-36]. The first part is the well-known Gilbert part, which leads to a linear dependence of linewidth with frequency. The second term takes the mosaicity of grains into account. Local variations of the sample parameters, such as the orientation of planes, variation of thickness or internal fields can lead to a superposition of different individual linewidths, including a field-dragging due to magnetic anisotropy effects of the sample. These first two parts are Gilbert-like, whereas the third one is the Two-Magnon Scattering (TMS) contribution. It is calculated by the scattering rate of the FMR mode ($k = 0$) to different spin wave modes ($k \neq 0$), including a frequency dependent term and a frequency independent term as well. The fourth and last part of the linewidth cannot be written in a Gilbert- or TMS-like form. It represents a frequency and angular independent broadening and can also be attributed to the zero frequency linewidth.

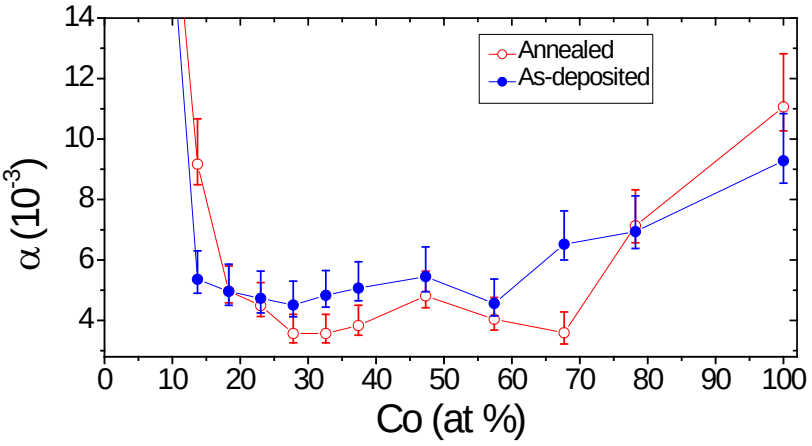

Figure 3: Comparison of the damping parameters of a full composition range of Co_xFe_{1-x}-alloys grown on Si substrate before and after annealing, extracted by a linear regression of equation 5. We obtain local minima of the damping at around 28 % and 57 %, respectively 68 % after annealing.

For our samples, we can see a correlation between the mosaicity and the residual linewidth and we thus identify mosaicity as the bulk of the contribution. Besides that inhomogenities such as imperfections of the lattice and interfaces like defects can add to the inhomogeneous broadening.

In Fig. 3, we present the evolution of the Gilbert damping parameters as a function of the Cobalt concentration for the samples grown on Si before and after post-annealing the films at 530 °C. In both cases, we observe a similar trend to the one measured by Schön et al.[17]. The minimal damping value we measured was at approximately 28 % Co. While in this first paper, only one minimum was found, our measurements indicate a local maximum at around 47 % Co and a second minimum at a Co percentage of 57. Afterwards, the damping increases again to a maximum for 100 % Co. When comparing the as-deposited and annealed samples we can clearly see a decrease in damping in the range between 28 % to 67 % Co, while an increase is exhibited for the Fe rich and the pure Co samples. We see that the lowest damping is for the annealed films also for 28 % Co, which is the same concentration as for the minimum in the as-deposited case and a second local minimum shifted to 68 % Co is found. This composition differs by around 10 % compared to the minimum in the as-deposited case. For the MgO and Al_2O_3 substrate samples only films with a Co composition of 28 % were annealed, showing the lowest magnetic damping, and we obtained a reduction of damping by 16 % and 24 %, respectively. Again the substrate does not seem to have a major impact on the magnetic damping. In contrast to the damping, no significant change of the resonance frequencies, i.e. the dispersion relations was recognized upon annealing, which leads to negligible changes in M_{eff} of less than 1 %. Furthermore, we extract the inhomogeneous linewidths, i.e. the frequency dependent linewidths extrapolated to zero frequency. We can conclude that sputter deposition in combination with annealing as post-treatment can result in even lower damping values than fabricating the samples by MBE[11]. Our results are summarized in Tab. 1.

Substrate	α_{eff} [10^{-3}]	$\Delta\mu_0 H_0$ [mT]	$\mu_0 M_{eff}$ [mT]	Annealing
Si	$(4.28 \pm 0.29\ [+0.38])$	0.62 ± 0.03	2357 ± 59	-
Si	$(3.61 \pm 0.22\ [+0.32])$	1.02 ± 0.03	2370 ± 60	X
Al_2O_3	$(4.78 \pm 0.32\ [+0.42])$	0.25 ± 0.03	2335 ± 59	-
Al_2O_3	$(3.74 \pm 0.26\ [+0.33])$	0.55 ± 0.02	2358 ± 59	X
MgO	$(4.77 \pm 0.32\ [+0.42])$	0.34 ± 0.03	2338 ± 59	-
MgO	$(3.63 \pm 0.25\ [+0.32])$	0.76 ± 0.03	2339 ± 59	X

Table 1: Comparison of damping on different substrates before and after annealing. We obtain a reduction of the effective Gilbert damping parameter by annealing with lowest value on Si substrate $(3.6 \pm 0.3) \cdot 10^{-3}$.

To understand the origin of the influence of annealing on the damping of our sample stack, we did several XRD measurements of the samples with lowest damping before and after annealing. On all substrates, the distribution of the orientation of the lattice planes narrowed during annealing by around 9 % to 15 %. As expected, also the grain size increased by a factor of 3 % to 8 %. These findings complement each other as being rooted in the improvement of magnetic homogeneity. So this means that by improving the crystallinity of our films, we can obtain a lower damping for post-annealed samples at a temperature of around 530 °C for a range of specific alloy compositions.

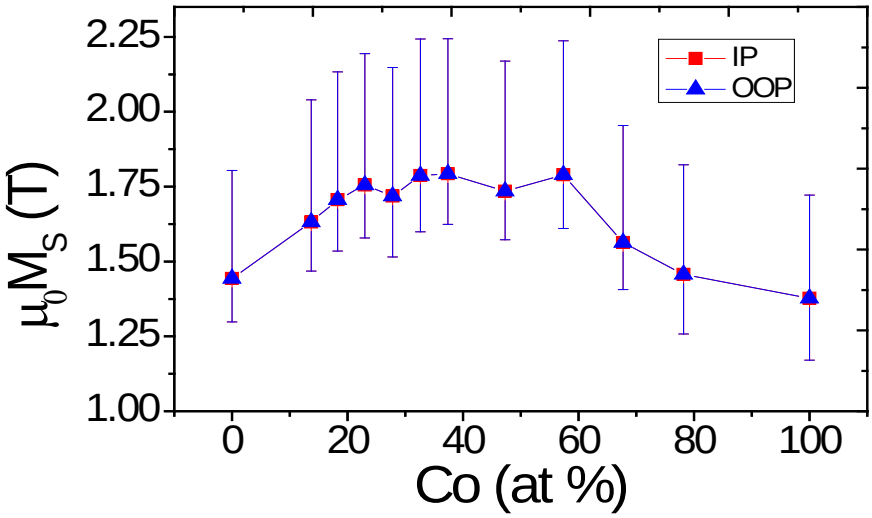

Figure 4: Values of the saturation magnetization of the Co_xFe_{1-x} stack in in-plane (IP) and out-of-plane (OOP) direction, being anti-correlated to the damping. The error bars are related to the accuracy in the determination of the volume of the ferromagnetic layer including statistical deviations. The asymmetry in the uncertainties is related to the calibration of the deposition rate by single layers, due to an uncertainty caused by oxidation, which contributed to the total thickness of the thin, uncapped calibration layer.

Last, we investigate the correlation between the magnetic damping and the saturation magnetization. In Fig. 4, we plot the saturation magnetization extracted from SQUID magnetometry in in-plane and out-of-plane fields. We observe a minimum saturation magnetization of (1.46 ± 0.34) T at 100% Co, a maximum for 57% with (1.80 ± 0.49) T, and a second local maximum (1.78 ± 0.45) T at 32%. For larger concentration of Fe, the saturation magnetization decreases again towards for the value of pure iron (1.46 ± 0.34) T. In line with previous work[17], we also observe a clear anti-correlation between saturation

magnetization and damping with two small discrepancies here. In contrast to previous work, we observe smaller saturation magnetization (1.78 ± 0.45) T at a composition of 32 % compared to reported values of (2.42 ± 0.05). This opposite trend between the magnetic damping and the saturation magnetization also explains the presence of a second minimum around 55 % in our study, as we observe a second local maximum of M_s for this concentration. The origin of this lower magnetization, however, needs still to be studied in a future work as it is beyond the scope of our current investigations.

IV. CONCLUSIONS

Ferromagnetic resonance measurements were done for a full composition range of 10 nm Co_xFe_{1-x} thin films sandwiched between 3 nm Cu and 3 nm Ta on Si (100) substrate. Additionally we have grown the compositions from 14 % to 37 % of the same stack on Al_2O_3 and MgO substrates, post-annealed the full composition range on Si at 530 °C and the $Co_{28}Fe_{72}$ composition on the other substrates as well.

We find a minimum of the damping at 25 % in line with previous work[17]. Growth on different substrates yields consistent results showing that the polycrystalline nature of the growth does not lend itself to be influenced by the substrate. The magnitude of our lowest damping value is consistent within the error bars to a previous in-plane measurement[20]. The evidence of this study shows a difference in the measured saturation magnetization for the full composition range. In contrast to previous work, find that additionally to the minimum around 25% there is a second local minimum at 57 % Co. We can explain this by the composition dependence of the saturation magnetization that exhibits at 57 % Co a second extremum in addition to the one around 25%.

To understand the origin of the damping variation, we carry out XRD measurements that show a large mosaicity and small grain sizes, typical for polycrystalline samples. Large inhomogeneous broadening of the FMR linewidths supports the assumption of sample imperfections governing the damping. For the post-annealed samples, we observe on one hand a clear decrease of the damping parameter for the lowest damping composition and on the other hand a significant increase of damping for the iron rich samples as well as the pure

Co. In our work we discuss the observed damping which after subtraction of two-magnon-, spin pumping- and small radiative damping contributions would lead to smaller intrinsic Gilbert damping values. We suppose advanced theoretical calculations considering the electronic structure of interfaces and its dependence on diffusion to be of major interest for a deeper understanding of the underlying influence of growth conditions, post-treatment and the choice of stack on the dynamical properties of the alloys in different measurement geometries.

ACKNOWLEDGMENTS

We acknowledge financial support by the European Community under the Marie Curie Seventh Framework program – ITN "WALL" (Grant No. 608031) and the Deutsche Forschungsgemeinschaft (DFG, German Research Foundation) - project number 268565370/TRR173. R.L. acknowledges the European Union's Horizon 2020 research and innovation programme under the Marie Skłodowska-Curie grant agreement FAST number 752195.

References

1. D. Kang and Y.-B. Kim, SoC for Internet of Everything (IoE), International SoC Design Conference and Institute of Electrical and Electronics Engineers and ISOCC, Piscataway, NJ, 61, (2015).

2. J. Heidecker, MRAM Technology Status, JPL Publication 13-3, Jet Propulsion Laboratory, California Institute of Technology, (2013).

3. J. Heidecker, Evaluation of magneto resistive RAM for space applications, JPL Publication 14-1, Jet Propulsion Laboratory, California Institute of Technology, (2014).

4. T. Dunn, A. Kamenev, Swing switching of spin-torque valves, Journal of Applied Physics 112 (10), 103906, (2012).

5. Tsymbal, E.Y. and D. Pettifor, Perspectives of giant magnetoresistance, Solid State Physics 56, 113, (2001).

6. C.-L. Wang, S.-H. Huang, C.-H. Lai, W.-C. Chen, S.-Y. Yang, K.-H. Shen, and H.-Y. Bor, Journal of Physics D: Applied Physics 42, 115006, (2009).

7. A. Mougin, M. Cormier, J. P. Adam, P. J. Metaxas, and J. Ferre, Europhysics Letters (EPL) 78, 57007, (2007).

8. A. A. Thiele, Physical review letters 30, 230, (1973).

9. P. Lai, G. P. Zhao, H. Tang, N. Ran, S. Q. Wu, J. Xia, X. Zhang, and Y. Zhou, Scientic reports 7, 45330, (2017).

10. S. Tsunegi, H. Kubota, K. Yakushiji, M. Konoto, S. Tamaru, A. Fukushima, H. Arai, H. Imamura, E. Grimaldi, R. Lebrun, J. Grollier, V. Cros, and S. Yuasa, Appl. Phys. Express **7**, 63009, (2014).

11. R. Lebrun, S. Tsunegi, P. Bortolotti, H. Kubota, A. S. Jenkins, M. Romera, K. Yakushiji, A. Fukushima, J. Grollier, S. Yuasa, and V. Cros, Nat. Commun. 8, (2017).

12. L. J. Cornelissen, J. Liu, R. A. Duine, J. B. Youssef, and B. J. van Wees, Nat. Phys. 11, 1022, (2015).

13. C. Schütte, J. Iwasaki, A. Rosch, and N. Nagaosa, Physical Review B 90, 101, (2014).

14. A. V. Chumak, V. I. Vasyuchka, A. A. Serga, and B. Hillebrands, Nat. Phys. 11, 453, (2015).

15. O. d'Allivy Kelly, A. Anane, R. Bernard, J. B. Youssef, C. Hahn, A. H. Molpeceres, C. Carrétéro, E. Jacquet, C. Deranlot, P. Bortolotti, R. Lebourgeois, J.-C. Mage, G. de Loubens, O. Klein, V. Cros, and A. Fert, Appl. Phys. Lett. 103, 82408, (2013).

16. C. Hauser et al., Sci. Rep. 6, 20827, (2016).

17. M. A. W. Schön, D. Thonig, M. L. Schneider, T. J. Silva, H. T. Nembach, O. Eriksson, O. Karis, and J. M. Shaw, Nature Physics 12, 839, (2016).

18. S. Mankovsky, D. Ködderitzsch, G. Woltersdorf, and H. Ebert, Physical Review B 87, 014430, (2013), 10.1103/Phys-RevB.87.014430.

19. I. Turek, J. Kudrnovský, and V. Drchal, Physical Review B 92, 214407, (2015), 10.1103/PhysRevB.92.214407.

20. H. S. Körner, M. A. W. Schön, T. Mayer, M. M. Decker, J. Stigloher, T. Weindler, T. N. G. Meier, M. Kronseder, and C. H. Back, Applied Physics Letters 111, 132406, (2017).

21. A. J. Lee, J. T. Brangham, Y. Cheng, S. P. White, W. T. Ruane, B. D. Esser, D. W. McComb, P. C. Hammel, and F. Yang, Nature communications 8, 234, (2017).

22. S.-F. Ding, S.-R. Deng, H.-S. Lu, Y.-L. Jiang, G.-P. Ru, D. W. Zhang, and X.-P. Qu, Cu adhesion on tantalum and ruthenium surface. Density functional theory study, Journal of Applied Physics 107 (10), 103534, (2010).

23. J. O. Rantschler, B. B. Mar, J. J. Mallett, P. Chen, R. D. McMichael, and W. F. Egelhoff, IEEE Transactions on Magnetics 41, 3523, (2005).

24. S. Azzawi, A. T. Hindmarch, and D. Atkinson, Journal of Physics D: Applied Physics 50, 473001, (2017).

25. J. Zhou, S. Chen, W. Lin, Q. Qin, L. Liu, S. He, and J. Chen, Journal of Magnetism and Magnetic Materials 441, 264, (2017).

26. G. Counil, J.-V. Kim, T. Devolder, C. Chappert, K. Shigeto, and Y. Otani, Journal of Applied Physics 95, 5646, (2004).

27. S. S. Kalarickal, P. Krivosik, M. Wu, C. E. Patton, M. L. Schneider, P. Kabos, T. J. Silva, and J. P. Nibarger, Journal of Applied Physics 99, 093909, (2006).

28. Y. Wei, S. Liang Chin, and P. Svedlindh, Journal of Physics D: Applied Physics 48, 335005, (2015).

29. M. A. W. Schön, J. Lucassen, H. T. Nembach, T. J. Silva, B. Koopmans, C. H. Back, J. M. Shaw, Phys. Rev. B 95 (13), (2017).

30. P. J. Mohr, D. B. Newell, and B. N. Taylor. CODATA recommended values of the fundamental physical constants: 2014. Reviews of Modern Physics, 88(3), 337, (2016), doi: 10.1103/RevModPhys.88.035009.

31. R. Arias and D. L. Mills, Physical Review B 60, 7395, (1999).

32. K. Zakeri, J. Lindner, I. Barsukov, R. Meckenstock, M. Farle, U. von Hörsten, H. Wende, W. Keune, J. Rocker, S. S. Kalarickal, K. Lenz, W. Kuch, K. Baberschke, and Z. Frait, Physical Review B 76, 133, (2007).

33. J. Dubowik, K. Za leski, H. Glowinski, and I. Goscianska, Physical Review B 84, 113, (2011).

34. H. Kurebayashi, T. D. Skinner, K. Khazen, K. Olejnik, D. Fang, C. Ciccarelli, R. P. Campion, B. L. Gallagher, L. Fleet, A. Hirohata, and A. J. Ferguson, Applied Physics Letters 102, 062415, (2013).

35. S. Jiang, L. Sun, Y. Yin, Y. Fu, C. Luo, Y. Zhai, and H. Zhai, AIP Advances 7, 056029, (2017).

36. J. F. Cochran, R. W. Qiao, and B. Heinrich, Physical Review B 39, 4399, (1989).

37. R. Weber, Spin dynamics in ferromagnetic alloys with low damping, Diploma Thesis, Institute of Physics, Johannes Gutenberg University Mainz, (2018).